Flatband Electroreflectance of Gallium Arsenide. II. Comparison of Theory and Experiment*

Stephen F. Pond† and Paul Handler
Department of Physics and Materials Research Laboratory, University of Illinois, Urbana, Illinois 61801
(Received 20 October 1972)

An analysis of previously reported electroreflectance (ER) data is presented. One-electron Franz-Keldysh-Aspnes (FKA) line shapes were compared to each ER structure observed in the 1.2–5.3-eV photon energy range. In addition, an excitonic theory of ER was compared to the direct edge data. We found it most useful to analyze the GaAs ER data by fitting FKA line shapes, considering the matrix elements thus obtained as exciton enhanced. The FKA fits determined the E_0 gap energy to be 1.427 ± 0.003 eV at 0 °C; the spin-orbit splitting at Γ, $\Delta_0 = 0.336 \pm 0.013$ eV. The interference between light- and heavy-hole transitions at E_0 was seen and the following quantities determined: light-hole reduced mass $\mu_{\rm lh} = (0.030 \pm 0.005)m_e$, heavy-hole reduced mass $\mu_{\rm hh} = (0.062 \pm 0.015)m_e$, and dipole matrix elements $C_{0\,\rm lh} = (1.16 \pm 0.2)\hbar/a_0$, $C_{0\,\rm hh} = (0.6 \pm 0.1)\hbar/a_0$, and $C_{0\,\rm soh} = (0.66 \pm 0.1)\hbar/a_0$. At the next-higher-energy structures, E_1, $E_1 + \Delta_1$, it was found that the two-dimensional FKA theory best represented the line shapes. The E_1 energy was found to be 2.884 ± 0.012 eV at 0 °C, and the spin-orbit splitting $\Delta_1 = 0.227 \pm 0.010$ eV. The reduced mass transverse to the [111] direction in $\vec{k}$ space was determined to be $\mu_t^{2D} = 0.053m_e$. Two structures in the 4.0–5.3-eV photon energy range were analyzed but remain poorly understood. A one-dimensional critical-point model is shown to be consistent with the highest-energy structure E'_0, but the structure is so broad that it can also be fit by other one-electron models.

I. INTRODUCTION

In a previous paper[1] we presented some new electroreflectance data for gallium arsenide. In that paper, hereafter denoted I, it was shown that the energy-band bending in the space-charge region was reliably characterized with respect to the flat-band (zero-space-charge) position. Extraction of minority carriers using an electrolyte electroreflectance (ER) technique made possible the achievement of nearly uniform fields. Further, it was found that the effects of thermal broadening, while present, were not dominating at most of the structures observed. These experimental conditions, discussed in I, are important to a successful quantitative analysis of ER data.

Electroreflectance spectra can usually be obtained with relative ease. The major problem is analyzing these spectra quantitatively. The theory of the optical properties in the presence of an electric field perturbation must be well understood. Quantities such as critical-point energies, spin-orbit splittings, effective masses, and dipole matrix elements can be extracted from the raw $\Delta R/R$ data of an ER experiment by fitting a theoretical line shape to the experimental spectra. The earliest attempted analysis of ER data, reported by Seraphin and Bottka[2] in 1966, was largely qualitative. They used peak energies to locate critical points and peak shifting with dc bias to differentiate parabolic and hyperbolic critical points. Since then the importance of field variation over the light penetration depth,[3,4] modulation in a field-on–field-off mode,[5] thermal broadening,[6] and the electron-hole Coulomb interaction (exciton)[7–9] has been understood. Different strategies have been developed to control these factors, or, at least, minimize their importance so that meaningful analysis can be performed on the experimental spectra. Transverse electroreflectance (TER), as performed by Rehn and Kyser,[10] emphasizes the attainment of uniform fields, low temperatures to minimize broadening, and varying field and light-polarization geometries. The experiment is intended to yield information about the symmetry of $\vec{k}$ space responsible for the observed spectra using the theory of Bottka and Fischer.[11] Linearized third-derivative spectroscopy, as performed by Aspnes and Rowe,[12] employs small surface-barrier fields and low temperatures. The data can then be analyzed using the relatively simple asymptotic forms[13] of the one-electron Franz-Keldysh-Aspnes theory.[14] The primary advantage of the technique is the ability to resolve nearly degenerate spectra. We have termed our strategy flat-band electroreflectance because the major emphasis is on modulating between the flat band and a large depletion or accumulation field. Near uniform fields are also important. The major shortcoming is the restriction to temperatures fairly close to room temperature, since an electrolyte technique is used. However, the data obtained by flat-band modulation and near uniform fields will determine more energy-band information than the other techniques previously mentioned.

In Sec. II we present an analysis of flat-band ER

data for GaAs based largely on the one-electron Franz-Keldysh-Aspnes[14] (FKA) theory. At the direct edge we have also used the exciton theory of Blossey.[8] An exciton theory was not applied above the direct edge because a detailed theory of ER for hyperbolic two- and one-dimensional excitons has not yet appeared. It will be seen in the following that the ER spectra at all energies can be fit by one-electron curves with reasonable consistency. However, some quantities, notably the dipole matrix elements, show large discrepancies with the same quantities determined by other experiments. The exciton theory can be made to fit the direct-edge data for a single surface-field value but does not give consistent results for a series of electric field strengths. Both the one-electron and exciton formulations used neglect field inhomogeneity effects, which were assumed small, and also the energy dependence of broadening.

In Sec. III we summarize the major claims and conclusions of this work.

II. COMPARISON OF THEORY AND EXPERIMENT

The data reported in I[1] covers the photon energy range 1.2–5.3 eV. In this range six definite structures are observed. They are discussed in Secs. IIIA–IIIC, which deal with the direct-edge structures E_0, $E_0+\Delta_0$, the Λ structures E_1, $E_1+\Delta_1$, and the uv structures E_0', E_2.[15] In I it was found from examination of the E_0 line shapes and collaborative capacitance measurements that quite uniform fields were obtained. The data was obtained using the electrolyte technique with potentiostatic control. The condition of zero surface field, flat band, was determined by utilizing the even-field-dependence property of the Franz-Keldysh effect. $\Delta\tilde{\epsilon}$ was obtained by a Kramers-Kronig transformation of $\Delta R/R$ and values of the optical constants were obtained by Eden.[16]

A. Direct-Edge Structures: E_0, $E_0+\Delta_0$

The ER structure seen in the 1.2–1.9-eV photon energy range for gallium arsenide arises from critical-point transitions from the three highest valence bands to the lowest conduction band at Γ. The highest valence state Γ_8 has a twofold orbital degeneracy which splits into a light-hole band and a heavy-hole band for $|\vec{k}|>0$ near Γ. Actually, because gallium arsenide lacks inversion symmetry, terms in the energy bands linear in $\vec{k}$ arise, shifting the valence-band maxima off Γ. These linear valence-band effects are small in GaAs[17] and have been neglected here. Thus the E_0 structure was considered the result of two degenerate M_0-type critical points at Γ. The next-higher-energy structure, $E_0+\Delta_0$, arises from the split-off valence band Γ_7, which is split from the Γ_8 band by an energy of $\Delta_0=0.336\pm0.013$ eV (this work).

The E_0 structure has been analyzed using both the one-electron theory and an exciton theory. In both cases it was found that the theoretical line shapes have enough flexibility to yield good fits to the data. Figure 1 shows the best one-electron and exciton fits to some moderately high-field ($\mathcal{E}\approx 7\times10^4$ V/cm) data.[1] Neither theory, however, yields parameters which are completely consistent with values for the same quantities calculated from other experiments. For example, the one-electron curve in Fig. 1 determined the light-hole dipole matrix element to be $C_{0\,\mathrm{lh}}=(0.92\pm0.1)\hbar/a_0$; whereas, a fit[18] of Elliot's[19] exciton theory to Sturge's[20] direct-edge absorption data gives a value of $0.39\,\hbar/a_0$ for the dipole matrix element. The exciton curve in Fig. 1 places the gap energy at 1.445 eV; whereas the fit[18] to Sturge's[20] absorption data gives a value of 1.437 eV.[21] A piezoreflectance experiment performed by Wells and Handler found a gap of 1.432 eV.[22]

The one-electron fits to the 7×10^4-V/cm data[1] and to some 1.3×10^5-V/cm data[1] are shown in Figs. 2 and 3. The field values quoted are actually derived from the fitting parameters used for the $E_0+\Delta_0$ structure. It was shown in I, however, that the field values determined in this way agree quite well with a calculation of the field using Poisson's equation and the known voltage used in the modulation. The dashed curves in Figs. 2 and 3 are plots of the following sum of FKA M_0 line shapes[13]:

$$\Delta\epsilon_1=\sum_j \frac{B_j}{\omega^2}\,G\left(\frac{\omega_j-\omega+i\gamma}{\theta_j}\right), \tag{1}$$

$j=$lh, hh, soh (light, heavy, and split-off holes), where

$$\theta_j=\left(\frac{e^2\mathcal{E}^2}{2\mu_j\hbar}\right)^{1/2}, \tag{2}$$

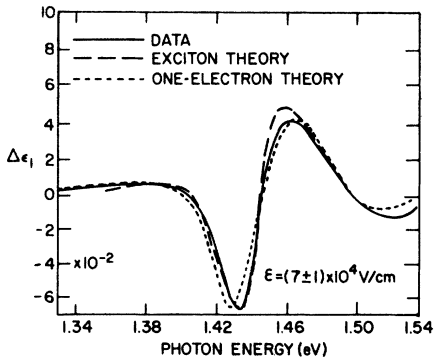

FIG. 1. Plot of the one-electron and exciton theoretical fits to the [001] polarization, 7×10^4-V/cm data of Paper I.

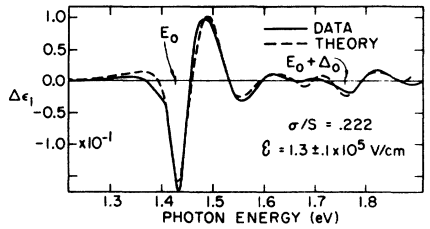

FIG. 2. Fit of FKA line shapes to the E_0, $E_0+\Delta_0$ structures of Fig. 2, paper I. The fitting parameters used in Eq. (1) were $\hbar^2\omega^2 A_l = 1.385$, $\hbar^2\omega^2 A_h = 1.182$, $\hbar^2\omega^2 A_{so} = 0.796$, $\hbar\omega_l = 1.427$ eV, $\hbar\omega_{so} = 1.763$ eV, $\hbar\theta_l = 60$ meV, $\hbar\theta_h = 47$ meV, $\hbar\theta_{so} = 52$ meV, $\hbar\gamma_l = 12$ meV, $\hbar\gamma_{so} = 20$ meV.

$$B_j = \frac{2e^2 C_{0j}^2}{m^2 h^2} \frac{8\mu_j \theta_j}{h^3} \quad , \tag{3}$$

$\mathcal{E}$ is the magnitude of applied electric field, μ_j is the reduced effective mass for the jth hole, and C_{0j} is the dipole matrix element for the jth valence band. Thus,

$$\gamma = \gamma_l + \frac{\gamma_{so} - \gamma_l}{\omega_{so} - \omega_l} (\omega - \omega_l). \tag{4}$$

$\hbar\gamma_{so}$ is the broadening at ($\hbar\omega_{so}$) in eV and $\hbar\gamma_l$ is the broadening at ($\hbar\omega_l$) in eV.

As can be seen in Eq. (4), thermal broadening was included as a linear function of photon energy. In practice the fits were accomplished by fitting the E_0 and $E_0+\Delta_0$ structures separately, then using these parameters as the starting values for Eq. (1). The convergence parameter used in all of our fitting programs was σ/S, the standard deviation of the difference between experimental and theoretical curves at each energy divided by the root-mean-square value of the experimental curve.

In order to present the results of the fits in terms common to other experiments, we assume that one of the reduced masses is known. From the literature we use a conduction-band mass[23] of $m_c = 0.067 m_e$ and a spin-orbit-split-off valence-band mass[24] of $m_{so} = 0.154 m_e$, obtaining $\mu_{so} = 0.0476 m_e$. With this value and the fitting parameters given in the caption of Figs. 2 and 3, the electric field $\mathcal{E}$, the dipole matrix elements, and other reduced masses are calculated. These quantities are given in Table I.

The FKA fits place the E_0 gap at 1.427 ± 0.003 eV (at 0 °C) and the $E_0+\Delta_0$ gap at 1.763 ± 0.011 eV (at 0 °C). The E_0 value is somewhat lower than that calculated from absorption data,[18,20,21] 1.437 eV, or piezoreflectance,[22] 1.432 ± 0.015 eV. The FKA value for the spin-orbit splitting at Γ was $\Delta_0 = 0.336 \pm 0.014$ eV. This value is in good agreement with the previously obtained values of 0.335 ± 0.020 eV from piezoreflectance[22] and 0.34 ± 0.01 eV from an early electroreflectance experiment.[25]

The fit to the 1.3×10^5-V/cm-field data shown in Fig. 3 determined the values for the light- and heavy-hole reduced masses to be $\mu_{lh} = (0.030 \pm 0.005) m_e$ and $\mu_{hh} = (0.063 \pm 0.015) m_e$. The errors given here were computed by considering the effect of errors in the fitting parameters and in m_c^*[23] and m_{so}^*[24] taken from the literature. These values for the masses compare favorably with determinations from other experiments. Interband magnetoabsorption experiments by Vrehen[23] determined $\mu_{lh} = (0.037 \pm 0.002) m_e$ and $\mu_{hh} = (0.058 \pm 0.002) m_e$. Intrinsic oscillatory photon conductivity experiments reported by Shaw[26] found $\mu_{lh} = (0.037 \pm 0.002) m_e$ and $\mu_{hh} = (0.060 \pm 0.002) m_e$. In the calculations reported here, as well as in those of Vrehen[23] and Shaw,[26] the conduction-band mass was taken to be $m_c^* = (0.067 \pm 0.002) m_e$, the value determined by Vrehen.[23]

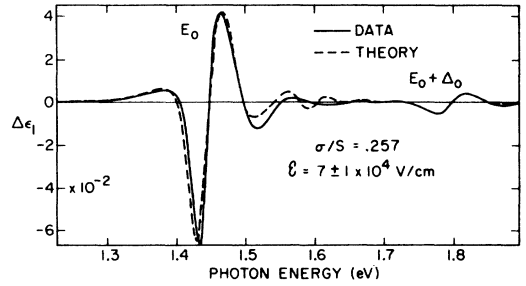

FIG. 3. Fit of FKA line shapes to the E_0, $E_0+\Delta_0$ structures, [001] polarization data of Fig. 4, Paper I. The fitting parameters use in Eq. (1) were $\hbar^2\omega^2 A_l = 0.7$, $\hbar^2\omega^2 A_n = 0.6$, $\hbar^2\omega^2 A_{so} = 0.5$, $\hbar\omega_l = 1.425$ eV, $\hbar\omega_{so} = 1.771$ eV, $\hbar\theta_l = 40$ meV, $\hbar\theta_h = 30$ meV, $\hbar\theta_{so} = 36$ meV, $\hbar\gamma_l = 10$ meV, $\hbar\gamma_{so} = 25$ meV.

TABLE I. Quantities calculated from the fits shown in Figs. 2 and 3. Values for some of the quantities obtained in other experiments are also given.

Quantity	This work		Other experiments	
Light-hole reduced mass (units of m_e)	0.030 ± 0.005	Fig. 3	0.037 ± 0.002	Ref. 26
	0.030 ± 0.005	Fig. 2	0.037 ± 0.002	Ref. 23
Heavy-hole reduced mass (units of m_e)	0.062 ± 0.015	Fig. 3	0.060 ± 0.002	Ref. 26
	0.070 ± 0.012	Fig. 2	0.058 ± 0.002	Ref. 23
Light-hole dipole matrix element ($\hbar/a_0$)	1.16 ± 0.2	Fig. 3	0.39	Ref. 18
	0.92 ± 0.1	Fig. 2	0.38	Ref. 27
Heavy-hole dipole matrix element ($\hbar/a_0$)	0.60 ± 0.1	Fig. 3		
	0.48 ± 0.1	Fig. 2		
Spin-orbit-split-off-hole dipole matrix element ($\hbar/a_0$)	0.66 ± 0.1	Fig. 3		
	0.56 ± 0.1	Fig. 2		

The matrix elements for the three interband transitions were also determined and are given in Table I. The one-electron theory gives values which are much too large, particularly the light-hole value as was mentioned previously. Part of the discrepancy between our computed values for the dipole matrix elements and the values obtained from the other experiments (see Table I) may lie in our calibration of $\Delta R/R$ and the conversion to $\Delta\tilde{\epsilon}$. The experimental $\Delta\tilde{\epsilon}$ curves may be as much as 20% too large because we assumed normal incidence of the light beam and no rounding of the square-wave modulation.

More importantly, the one-electron theory is simply not a complete description of the experiment. Exciton contributions are known to be important[27] and should be included in some way. Blossey[8] and Weinstein, Dow, and Lao[9] have included exciton effects by solving the revelant Schrödinger equation numerically. They have thus been able to discuss the role of exciton effects in electroreflectance. The essential differences of the excitonic theory as compared to the one-electron are[9] (i) a larger magnitude, (ii) a shift of the spectrum to lower energy, and (iii) a narrower, sharper first negative peak. These differences, of course, depend on the applied-field strength and the size of the thermal broadening. If the broadening is much above one exciton rydberg, the exciton bound states become ionized and contribute little to electroreflectance. However, the continuum exciton states above the energy gap are still important, as can be seen in Fig. 3 of Weinstein *et al.*[9] If the broadening-to-exciton-rydberg ratio is very large (greater than 30) then the one-electron theory and exciton theory become nearly the same. With direct-edge rydbergs of 3.22 and 5.17 meV for the light and heavy holes, such a large broadening-to-exciton-rydberg ratio is not observed at the direct gap, but may be approached for the higher-energy structures observed in GaAs and other semiconductors.

The exciton-theory curve in Fig. 1 was constructe by hand from Figs. 10 and 11 of Blossey's paper.[8] That is, the curve is sketched in after determining the zeros, peak heights, and approximate peak positions. The procedure was to construct separate curves for the light- and heavy-hole excitons, using literature values for the masses, dipole matrix elements calculated from other experiments,[18,28] field strength and broadening from the one-electron fits, and a variable gap energy. The values of the parameters used in constructing the exciton line shape in Fig. 1 are given in the figure caption. This fit is really quite satisfying, with the exception of the determined energy-gap value, 1.445 eV, which is 7–10 meV higher than that found in other experiments.[18,22] However, such generally good agreement cannot be found consistently over several different field values. Fig. 4 shows the exciton fit to the data of Fig. 3. This fit was obtained using the 1.3×10^5-V/cm field value obtained from the one-electron fit, and all other parameters were the same as those used for the exciton curve of Fig. 1. The agreement between curves in Fig. 4 could be improved by assuming a field strength twice as large as that used. The field cannot have been that large, however. An application of Poisson's equation[1] gives a value of $\mathcal{E} = 1.1\times10^5$ V/cm for the data as compared to the 1.3×10^5 V/cm obtained from the one-electron theory.

The exciton theory, as currently formulated by Blossey[8] and Weinstein *et al.*[9] is difficult to apply because of the complicated computer routines necessary. In view of this, and since the exciton theory does not give consistent results for a series of field strengths, it is useful to continue to use the simpler one-electron theory for high-field data and include exciton effects as merely an enhancement of the dipole matrix element. This approach is justified by Blossey's findings about the exciton theory.[8,29] Blossey calculated exciton absorption in an electric field in the effective-mass approximation, using parabolic coordinates. He found that each bump or oscillation in the electric field absorption spectrum above the direct gap corresponds to a parabolic coordinate eigenvalue and that this was also the case for the one-electron approach.[29] The net result is that for large fields ($\hbar\theta \gg \epsilon_x$, the exciton rydberg), the exciton and one-electron theories give similar results for the location in energy of the oscillations above the gap, but the amplitude of the oscillations is considerably larger in the exciton theory. We have plotted an enhancement factor D in Figure 5. This factor is the ratio of the maximum value of $|\Delta\epsilon_1|$ in the exciton theory to the maximum in the one-electron theory. The values

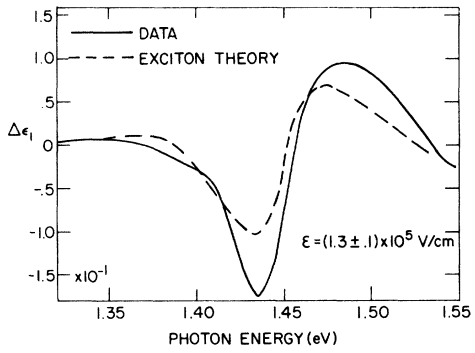

FIG. 4. Exciton fit of the same data shown in Fig. 3. The exciton curve was constructed using the results of Blossey's calculations (Ref. 8). The exciton curves in Fig. 1 and above use the same values for the exciton Rydberg, 4.2 meV, the dipole matrix element, $0.39\,\hbar/a_0$, and the E_0 energy gap, 1.445 eV.

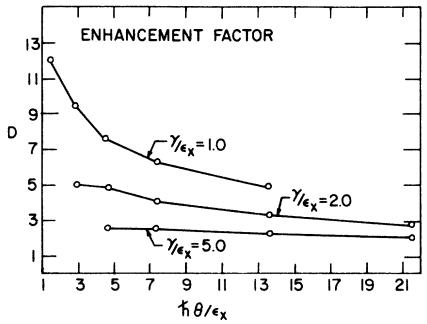

FIG. 5. The apparent enhancement D of the one-electron dipole matrix element by the exciton. D is the ratio of $|\Delta\epsilon_1|$ in the exciton theory [from Fig. 11 of Blossey's paper (Ref. 8)] to $|\Delta\epsilon_1|$ in the FKA theory. For large broadening-to-rydberg ratios this enhancement becomes almost independent of applied-field strength.

for $|\Delta\epsilon_1|_{max}$ in the exciton theory were obtained from Fig. 11 of Blossey's paper.[8] Figure 5 shows that as the broadening increases the enhancement becomes smaller and rather constant with respect to the $\hbar\theta/\epsilon_x$ ratio. For the situations of Fig. 3 the curves of Fig. 5 predict enhancements of from 2.5 to 4.0 for the various exciton contributions. This corresponds to an enhancement of the apparent dipole matrix element of 1.6–2.0.

A final important factor to consider in evaluating the theoretical fits shown above is field inhomogeneity.[3] In the previous paper, I, we discuss field inhomogeneity and concluded that for our data the effects were small. However, there is still some diminution of subsidiary oscillations in $\Delta\tilde{\epsilon}$, caused by field inhomogeneity.[13] Since the FKA and exciton theories are for uniform fields, the broadening parameters in the fits will turn out too large in order to account for some of the field-inhomogenity effects. This in turn will necessitate a larger fitting amplitude, hence a larger dipole matrix element. We used broadening energies of 10 and 12 meV for Figs. 2 and 3, respectively. A fit of Sturge's[20] room-temperature absorption data using the method of Sell and Lawaetz[18] gives a value of 8 meV for the room-temperature broadening. Because the maximum peak heights of the electro-optic F and G functions vary so rapidly for $\gamma/\hbar\theta$ small, an error of only 4 meV in the direct-edge-broadening parameter can result in a 20% error in the fitting amplitude. Thus slight field inhomogeneity, by making the oscillations diminish more rapidly, contributes to error in the broadening energy and also in the dipole matrix element.

The quantitative agreement between the one-electron and exciton theories, and experiment is fair. Both theories can be made to fit the data; however, neither, is completely consistent with other experimental results. The practical approach to analyzing high-field moderate-broadening electroreflectance data is to use the Franz-Keldysh-Aspnes theory,[13] including exciton effects as an enhancement of the dipole matrix element. The failure of the current exciton theories to consistently fit a series of ER line shapes taken with different field values indicates that a better theoretical understanding of electroreflectance must yet be sought.

B. Λ Structures: E_1, $E_1+\Delta_1$

There has been considerable controversy over the type and location in $\vec{k}$ space of the critical points responsible for the 2.6–3.4-eV structure in GaAs electroreflectance spectra shown in Fig. 6, as there has been over the corresponding structures in other zinc-blende and diamond semiconductors. Initially, when band-structure calculations were limited to high-symmetry points in the Brillouin zone, this structure was attributed[30] to direct transitions of M_0^{3D} type at the L point ($L_3'\rightarrow L_1$) which is located at the zone boundary, $\vec{k}=0.5(1, 1, 1)$. In 1962, Brust *et al.*[31,32] extended the calculations for Ge to the entire Brillouin zone. Their calculations indicate the existence of an M_1^{3D} critical-point pair near 0.17(1, 1, 1) with an energy gap of the order of the E_1, $E_1+\Delta_1$ transitions, and place the M_0^{3D} L-point transitions at a lower energy. Largely on the basis of these calculations, the E_1, $E_1+\Delta_1$ structures were classified as a spin-orbit-split pair of M_1^{3D} critical points and the predicted M_0^{3D} pair sought experimentally at lower energies.

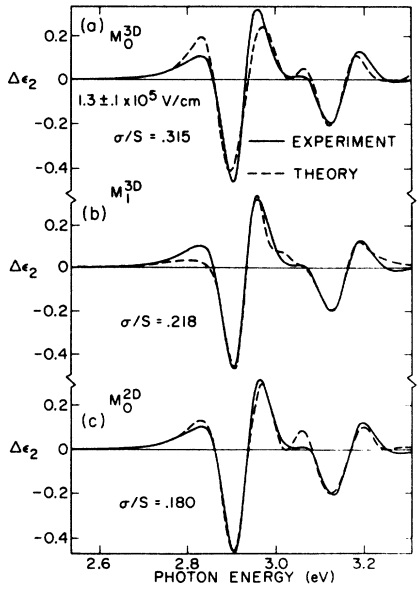

FIG. 6. The fits of three different FKA theories to the 1.3×10^5-V/cm $\Delta\epsilon_2$ curve of Fig. 8 in Paper I. The fitting parameters are given in Table II.

Reflectance work by Potter[33] in Ge and Greenaway and Cardona[34] in GaAs has shown a pair of modest shoulders below the large E_1, $E_1+\Delta_1$ peaks which were tentatively assigned to the M_0^{3D} transitions at the L point. More recent reflectance work by Sell and Stokowski[35] on GaAs has found that these weak features are not characteristic of the reflectance of good-quality surfaces of pure GaAs. Furthermore, none of the recent modulation experiments on GaAs or Ge have ever shown more than one apparent pair of critical points in this energy region.

More recent band-structure calculations by Dresselhaus and Dresselhaus[36] on Ge found several doublet critical points along Λ, all having transition energies very close to the E_1, $E_1+\Delta_1$ energies. In addition they find the transitions at the L point to be of the M_1^{3D} type rather than of the M_0^{3D} kind. Empirical pseudopotential calculations by Zucca *et al.*[37] on GaAs found M_0^{3D} transitions at L with an energy of 2.82 eV and M_1^{3D} transitions [0.2(1, 1, 1) in $\vec{k}$ space] with an energy of 3.02 eV.

In view of all this, it is evident that the band-structure calculations and the experimental evidence are not precise enough to identify the E_1, $E_1+\Delta_1$ transitions in GaAs as M_1^{3D} and not M_0^{3D} or *vice versa*. Indeed, it may well be that the transitions observed do arise from both M_1^{3D} and M_0^{3D} critical points nearly degenerate in energy, as has been suggested by Aspnes and Rowe[38] for Ge. Trying to fit two or more critical-point pairs to the observed electroreflectance line shapes is impractical, however, because of the large number of fitting parameters involved in such an approach. The data in Fig. 6 do not contain enough oscillations to determine so many parameters uniquely. A useful approximation in this situation is to consider $\vec{k}$ space in the region along Λ to be two-dimensional from the L point quite far in towards Γ.[39,40]

An attempt has been made to fit the $\Delta\epsilon_2$ curves of Fig. 8 in Paper I to each of the three types of critical points which are suggested by the theoretical band calculations, and M_0^{3D} pair, an M_1^{3D} pair, and an M_0^{2D} pair. Typical results of these three different one-electron theories are shown in Fig. 6 for the 1.3×10^5-V/cm data. Each of the fits shown assumed that the structure was a spin-orbit-split pair, hence two electro-optic functions were needed. The transitions $(\Lambda_4^v+\Lambda_5^v)\rightarrow\Lambda_6^c$, $\Lambda_6^c\rightarrow\Lambda_6^c$, were assumed to have equal dipole matrix elements and effective mass, hence equal amplitudes and values of $\hbar\theta$ at a given field. These assumptions reduced the number of parameters from eight (four for each critical point) to six: one amplitude, one $\hbar\theta$, two energy gaps, and two values of constant broadening. Thus the dashed curves of Fig. 6 are plots of the following theoretical expressions for $\Delta\epsilon_2$:

$$M_0^{3D}:\ \Delta\epsilon_2 = A^{3D}\left[F_3\left(\frac{\omega_1-\omega+i\gamma_1}{\theta}\right)+F_3\left(\frac{\omega_2-\omega+i\gamma_2}{\theta}\right)\right], \quad (5)$$

$$M_1^{3D}:\ \Delta\epsilon_2 = A^{3D}\left[G_3\left(\frac{\omega_1-\omega+i\gamma_1}{\theta}\right)+G_3\left(\frac{\omega_2-\omega+i\gamma_2}{\theta}\right)\right], \quad (6)$$

$$M_0^{2D}:\ \Delta\epsilon_2 = A^{2D}\left[F_2\left(\frac{\omega_1-\omega+i\gamma_1}{\theta}\right)+F_2\left(\frac{\omega_2-\omega+i\gamma_2}{\theta}\right)\right], \quad (7)$$

where $h\omega_1$ is the energy of E_1, $h\omega_2$ is the energy of $E_1+\Delta_1$, $\hbar\gamma_1$ is the constant thermal broadening at E_1, and $\hbar\gamma_2$ is the constant thermal broadening at $E_1+\Delta_1$. Thus,

$$A^{3D} = \frac{2e^2C_0^2}{m^2\omega^2}\left(\frac{8\mu_t^2\mu_\parallel}{\hbar^6}\right)^{1/2}(\hbar\theta)^{1/2}\nu, \quad (8)$$

$$A^{2D} = \frac{2e^2C_0^2}{m^2\omega^2\hbar}(\mu_t)\Delta k\nu, \quad (9)$$

where ν is the factor to account for the number of equivalent regions in the Brillouin zone, Δk is the length in k-space of the parallel region in the two-dimensional theory, and μ_t is the effective mass transverse to the direction of parallelicity.

Table II presents the parameters which gave the best fit for each of the three theories. The last column gives the value of the fitting criterion used by the computer program, σ/S.

Actually, the situation is more complicated than indicated by Eqs. (5)–(7). The data is for a [110] field direction and the transitions occur along the eight equivalent Λ directions. This means that half the ellipsoids will experience one field strength and half another. It has been shown elsewhere[41] that for thermal broadenings of the size encountered here, Eqs. (5)–(7) are adequate provided the factor ν is used to adjust for the proper contributions of the two sets of ellipsoids (cylinders in the two-dimensional approach).

The M_0^{2D} theory was the most successful of the three as can be seen by examining Fig. 6. The fitting program converged rapidly to a value of $\sigma/S=0.180$. The theoretical curve reproduces the leading positive peak very well, which is quite important since it is mostly unaffected by the spin-orbit-split-off structure. If field inhomogeneity is small the leading edge of $\Delta\epsilon_2$ will easily distinguish between relevant F and G functions, as it does in the curves of Fig. 6. The M_1^{3D} fit was also good, having a σ/S value of 0.218, but it does not do very well on the leading edge. The M_0^{3D} fit

TABLE II. Fitting parameters used in Eqs. (5)–(7) to produce the theoretical curves shown in Figs. 6 and 8.

Fig.	Theory	Field (10^5 V/cm)	$\hbar^2\omega^2A$	E_1 (eV)	$E_1+\Delta_1$ (eV)	$\hbar\theta$ (meV)	$\hbar\gamma_1$ (meV)	$\hbar\gamma_2$ (meV)	σ/S
6(a)	M_0^{3D}	1.3 ± 0.1	44.0	2.860	3.081	61.6	24.8	41.8	0.315
6(b)	M_1^{3D}	1.3 ± 0.1	497.3	2.914	3.142	30.0	46.9	63.7	0.218
6(c)	M_0^{2D}	1.3 ± 0.1	109.6	2.884	3.111	49.7	49.0	66.6	0.180
8(b)	M_0^{2D}	1.0 ± 0.1	109.6	2.888	3.111	41.7	49.0	66.6	0.231
8(c)	M_0^{2D}	0.5 ± 0.2	109.6	2.895	3.118	24.0	49.0	66.6	0.344

in Fig. 6 represents the best that could be obtained after repeated adjustments of the starting values of the six parameters of Eq. (5). The fit shown has a σ/S value of 0.315. The fitting program would not converge to a better fit, and in fact diverges to worse fits than that of Fig. 6. This is in contrast to the situation found in Ge, where the M_0^{3D} theory does give a good convergent fit.[42]

It is interesting that an M_1^{3D} theory does fairly well for GaAs but not an M_0^{3D} theory; whereas the opposite is true for Ge.[42,43] This indicates a subtle difference between GaAs and Ge band structures along Λ. Remembering that the two-dimensional model is an approximation to a situation of multiple critical points, it seems that for GaAs the portion of k space along Λ with negative curvature exceeds the portion with positive curvature, and *vice versa* for Ge.

Although the M_1^{3D} fit in Fig. 6 looks fairly good, the fitting parameters determined contradict one of the basic assumptions of the FKA theory, parbolic bands over the photon energy range being considered. We can see this contradiction by deriving the value of $\mu_{\parallel}$, the effective mass along the [111] direction. Using the expression for θ in Eq. (2), assuming that the transverse mass μ_t is dominant, one finds $\mu_t = 0.243m_e$ ($+0.104m_e$, $-0.072m_e$). With this value one obtains $\mu_{\parallel} = 213m_e$ from the fit parameters given in Table II and the expression for A^{3D} in Eq. (8) (ν was taken to be 5.52[41] and $C_0 = 1.0\hbar/a_0$). An effective mass of $213m_e$ is extremely large, casting doubt on the validity of the parabolic band assumption. If the bands were parabolic over the entire region along Λ, that is, for $|\vec{k}_{111}|$ from 0.0 to 0.5 a.u., the parabolic-band assumption would limit the validity of the theory to photon energies less than 12 meV above the critical-point energy. This is much too narrow a range for the observed line shapes.

The amplitude fitting parameter in the M_0^{2D} fits carries information about the dipole matrix element $(C_0)^2$ and the length of the 2D region, $\Delta\vec{k}$, along the critical line. This can be seen from Eq. (9), $\hbar^2\omega^2A^{2D} \propto C_0^2\,\Delta k\,\mu_t^{2D}$. The transverse effective mass μ_t^{2D} is determined by the $\hbar\theta$ fitting parameter and the value of the electric field obtained from the fits at the $E_0+\Delta_0$ structure. From the fitting parameters for Fig. 6(c) given in Table II it is found that $\mu_t^{2D} = 0.053m_e$ ($+0.016m_e$, $-0.012m_e$). Using this value in Eq. (9) along with $\hbar^2\omega^2A^{2D} = 110$, $\hbar\theta = 49.7$ meV, and $\nu = 5.52$,[41] the product $(C_0^2)(\Delta k_{111})$ can be determined. Neither of these two quantities has been determined individually by experiment, so to say anything further one must use one-electron band-theory calculations. An energy-band diagram by Zucca *et al.*[37] for GaAs is shown in Fig. 7. The suspected region extends about 70% of the way from L to Γ along Λ, indicating a Δk_{111} of about 0.35 a.u. $\Delta k_{111} \simeq 0.35$ a.u. implies that $C_0 \simeq 0.84\,\hbar/a_0$. This value is larger than would be expected from the values obtained in other experiments[28] at the direct edge. As was discussed in Sec. II A, some of the discrepancy may be due to experimental assumptions. However, a part may also be due to exciton enhancement. The problem of exciton absorption at a two-dimensional edge (or hyperbolic critical point) has not been solved exactly. A con-

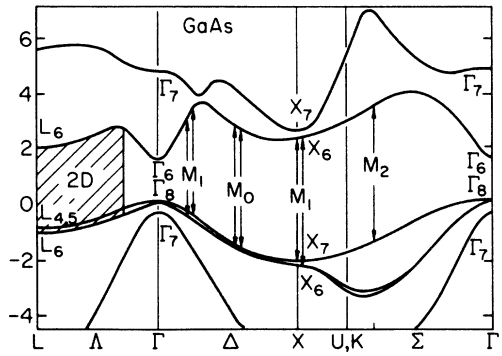

FIG. 7. Energy bands for GaAs by Zucca *et al.* (Ref. 36). We have indicated the two-dimensional region along Λ responsible for the E_1, $E_1+\Delta_1$ structures. Also indicated are possible transitions responsible for the E_0', E_2 structures.

tact-exciton-interaction approximation has been formulated.[44] We did not apply this approximation to our data because to do so would require introducing another adjustable parameter in the fitting procedure. The data does not contain enough structure to profitably determine more fitting parameters.

As a final test of the 2D theory it is shown that the fitting parameters obtained at the highest-field data can be used to fit data obtained at other fields. This has been done for the three $\Delta\epsilon_2$ curves of Fig. 8 of Paper I. First, a fit of the highest-field curve was done letting all six parameters vary. Then the two lower-field curves were fit using these same six parameters, adjusted by the values of the electric field obtained from the $E_0 + \Delta_0$ structure. The results of this procedure are shown in Fig. 8; the fitting parameters tabulated in Table II. The fit becomes worse as the field decreases as can be seen from the σ/S values in Table II and the trend of Fig. 8. This is in accord with the fact that energy-dependent broadening and exciton effects, which were not taken into account, become less important at higher fields as $\hbar\theta$ becomes larger relative to $\hbar\gamma$, the broadening and ϵ_x, the exciton rydberg.

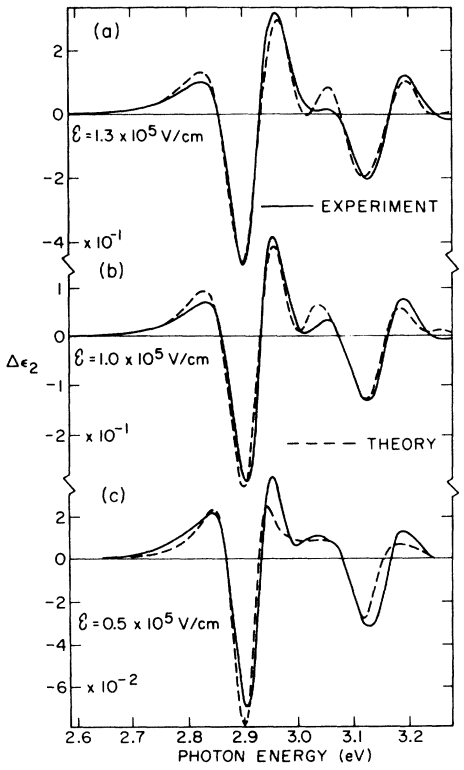

FIG. 8. M_0^{2D} fits to the three $\Delta\epsilon_2$ curves of Fig. 8 of Paper I, using the same parameters for the lower two fields as were determined by the fit at the highest field. $\hbar\theta$ was adjusted by the known field values and the energy gaps were allowed to vary within the 12-meV uncertainty limits. The parameters used in Eq. (7) for these fits are given in Table II. Figure 8(a) is identical to Figure 6(c).

The fits shown in Fig. 8 determine a critical-point energy $E_1 = 2.884 \pm 0.012$ eV (at 0 °C) and a spin-orbit splitting of $\Delta_1 = 0.227 \pm 0.010$ eV. Spin-orbit splitting arises from triply degenerate p-like valence-band states. At the zone center, $\vec{k} = 0$, the spin-orbit interaction breaks this degeneracy into a quadruplet (light- and heavy-hole Kramers degenerate bands) and a doublet (Kramers degenerate split-off valence band) separated by an energy Δ_0. Off Γ along a direction in $\vec{k}$ space with at least threefold symmetry, the quadruplet is further split by the spin-orbit interaction by an amount $\Delta_1 = \frac{2}{3}\Delta_0$, if Δ_1 is small compared to the $\vec{k}\cdot\vec{p}$ splitting.[15] Comparing the determined value of Δ_1 just given with that of Δ_0 found previously one obtains $\Delta_1/\Delta_0 = 0.676$, in good agreement with the two-thirds rule. An additional parameter which is well determined is the reduced mass transverse to the [111] direction, $\mu_t^{2D} = 0.053m_e$ $(+0.016m_e, -0.012m_e)$.

On the whole, the M_0^{2D} theory provides a remarkably good understanding of the GaAs E_1, $E_1 + \Delta_1$ spectra. The two-dimensional approach is well justified by current band-structure calculations. The computer fits have low σ/S values, and the parameters are self-consistent over a reasonable field range. The true situation may well be one of multiple critical points. An examination of the M_0^{3D} and M_1^{3D} theoretical curves of Fig. 8 suggests that a simple linear combination of M_0^{3D} and M_1^{3D} critical points would give a rather good fit. Unfortunately, such an approach is impracticable in view of the large number of parameters already involved and the small number of oscillations in the experimental curves. Thus, the two-dimensional critical-point theory is a more useful approach and has been successful for Ge[43] and GaAs. This interpretation of the local band structure along the Λ line should be reasonably accurate in most diamond–zinc-blende semiconductors.

C. 4.0–5.3-eV Region: E_0', E_2

The electroreflectance data reported in I[1] shows structure in the 4.0–5.3-eV photon energy range. The structure in the 4.0–5.3-eV region is usually labeled E_0' and that near 4.9 eV, E_2.[45] The location in the Brillouin zone of these and the corresponding transitions in other diamond–zinc-blende semiconductors is still not known very well. We have performed an analysis of our data by trying to fit all possible one-electron line shapes to the $\Delta\epsilon_2$ spectra shown in Figs. 9 and 10 of Paper I.[1]

Consider first $\Delta\epsilon_2$ shown in Fig. 9 for the E_2

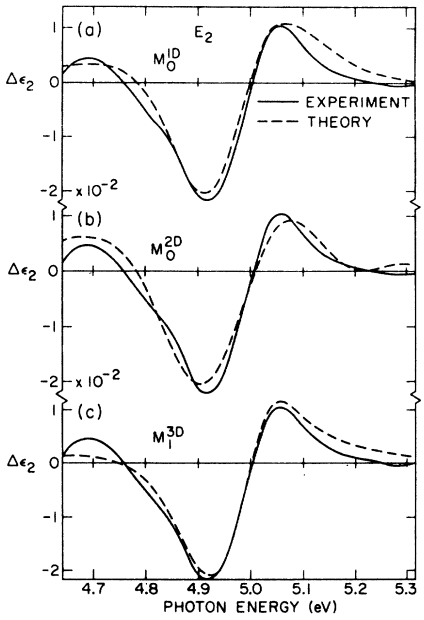

FIG. 9. The fits of three different FKA theories to the 1.6×10^5-V/cm $\Delta\epsilon_2$ E_2 curve of Fig. 9 of Paper I. The parameters for these fits are given in Table III.

structure taken with the field in the [110] direction. Three different types of critical points were found to fit the data about equally well, a one-dimensional M_0^{1D}, a two-dimensional M_0^{2D}, or a three-dimensional M_1^{3D}. These three fits are shown in Fig. 9 and the parameters are given in Table III. Some of the parameters vary greatly among the three different fits. The broadening in particular varies from 138 to 210 meV for the fits. Since an adequate theory of the photon energy dependence of broadening has not yet been developed, one cannot say which, if any, of the broadening values are reasonable. Hence there is insufficient evidence to conclude *a priori* which theory best represents the line shapes at E_2.

The one-dimensional model suggested by the good fit obtained with an M_0^{1D} can be justified by the apparently large volume of k space contributing to the E_2 transitions.[45,46] Also, Cardona and Pollak[47] have recently applied the Penn model, a simple model of an insulator based on one-dimensional bands, to the case of diamond–zinc-blende semiconductors. They found that most optical properties of these materials were qualitatively accounted for by their simple model composed of a one-dimensional M_0^{1D} critical point at E_2 (the Penn gap), an M_0^{2D} pair of critical points at E_1, $E_1+\Delta_1$, and a three-dimensional M_0^{3D} critical point at the direct edge. It is interesting to calculate the size of the one-dimensional region implied by the fitting parameters in Table III.

TABLE III. Fitting parameters used in the theoretical expressions to produce the curves of Fig. 9.

Fig.	Theory	$\hbar^2\omega^2A$	E_2 (eV)	$\hbar\theta$ (meV)	$\hbar\gamma$ (meV)	σ/S
9(a)	M_0^{1D}	142.9	4.951	75.0	211.0	0.236
9(b)	M_0^{2D}	31.7	4.868	118.4	169.6	0.212
9(c)	M_1^{3D}	34.6	4.947	62.3	138.0	0.212

The dashed curve in Fig. 8(a) is a plot of

$$\Delta\epsilon_2 = A^{1D}F_1\left(\frac{\omega_g-\omega+i\gamma}{\theta}\right), \tag{10}$$

$$A^{1D} = \frac{e^2C_0^2}{\pi m^2\hbar\omega^2}\left(\frac{2\mu}{\hbar\theta}\right)^{1/2}(\Delta k)^2\nu\,, \tag{11}$$

where $(\Delta k)^2\nu$ is the effective area of $\vec{k}$ space which is one-dimensional and all the other quantities are as they have been described previously. F_1 is the one-dimensional electro-optic function.[13] From the fitting parameters in Table III, it is found that $(\Delta k)^2\nu = 0.18$ a.u. (units of $1/a_0^2$). This 0.18-a.u. area includes all of the equivalent locations in the Brillouin zone at which the field has a projection parallel to the finite-mass direction. A plane through the entire Brillouin zone (BZ) would have an area of about 0.85 a.u. The matrix element C_0^2 in Eq. (11) was taken to be 1.0 a.u., which may be much too large. Cahn and Cohen[46] have published contours of $\vec{k}$ space for GaSb which show plateau regions with a total area of about 0.4 a.u. per Brillouin zone at the E_2 energy. Thus the value obtained for $(\Delta k)^2\nu$ seems reasonable, and the one-dimensional critical-point model is at least consistent with our E_2 data.

The E_0' structure, shown in Fig. 10, is potentially more complicated than the E_2. Wavelength-modulation experiments[37,48] conducted at 5 °K show a closely spaced doublet in the E_0' region with critical-point energies at 4.44 and 4.60 eV. In the room-temperature wavelength-modulation

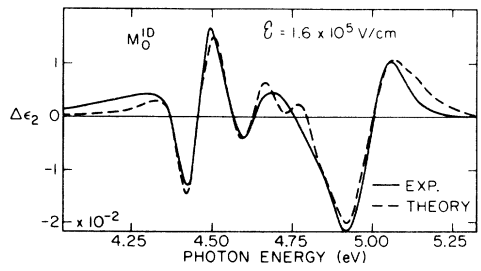

FIG. 10. M_0^{1D} fit to both E_0' and E_2 structures for the 1.6×10^5-V/cm $\Delta\epsilon_2$ curve of Fig. 9 of paper I. The E_0' parameters used in Eq. (10) were $\hbar^2\omega^2A = 1.80$, $\hbar\omega_g = 4.415$ eV, $\hbar\theta = 76$ meV, $\hbar\gamma = 52$ meV. The E_2 parameters used in Eq. (10) were $\hbar^2\omega^2A = 141.6$, $\hbar\omega_g = 4.951$ eV, $\hbar\theta = 75$ meV, $\hbar\gamma = 210$ meV.

data[37,48] this doublet is not resolved.

Little success has been achieved in fitting the $\Delta\epsilon_2$ line shapes to the possible one-electron theories suggested by the wavelength-modulation results and the band calculations.[37,46,48] The predicted[37,48] situation along Δ of multiple critical points suggests an M_0^{2D} pair at 4.425 and 4.60 eV. The best that could be done with this approach was a fit with $\sigma/S = 0.6$, which is not very good. The large posivite peak in $\Delta\epsilon_2$ at 4.5 eV, the narrowness of both negative peaks coupled with the ratio of 3:1 between them, and the proximity of the other structure at 4.9 eV are the features which could not be fit simultaneously. A single M_0^{1D} critical point will fit reasonably well, $\sigma/S = 0.268$. This fit plus the best M_0^{1D} fit at E_2 are plotted in Fig. 10. The parameters of the fit are given in the caption of the figure. The fit places the critical point at 4.415 eV. This fit is presented because it is the only one-electron FKA line shape which will fit the E_0' data at all well. There are, however, certain contradictions evident in the two sets of parameters for the two structures involved in Fig. 10. The E_0' amplitude factor is two orders of magnitude smaller than the E_2 amplitude factor, implying a region of $\vec{k}$ space which would be rather small to consider as a one-dimensional plateau. Second, the broadening came out to be only 52 meV at E_0' compared to 67 meV at $E_1+\Delta_1$ and 210 meV at E_2. Although the energy dependence of the broadening is not understood very well, it is expected to be monotonic with photon energy.

This energy region must be investigated at lower temperatures[49] and the energy dependence of broadening better understood before the E_0' and E_2 structures can be properly located in the Brillouin zone. Also work in other materials at these structures is needed to provide additional clues to the $\vec{k}$-space origin of these transitions.

III. CONCLUSIONS

We have presented an analysis of the flat-band electroreflectance data previously reported.[1] Experimental conditions were chosen so as to most closely approximate the situation assumed in the derivation of the one-electron Franz-Keldysh-Aspnes theory, i.e., uniform electric fields, large in magnitude with respect to the exciton ionization field,[8] and modulation from the flat band. A detailed analysis was performed on each observed structure by fitting on FKA line shapes to the experimental curves. In addition, Blossey's exciton theory[8] was applied to the E_0 line shapes.

At the direct edge, a good fit could be obtained with either the FKA or the exciton theories, provided sufficient flexibility in the fitting parameters was allowed. The FKA theory gives obviously poor values for the dipole matrix elements. The exciton theory is inconsistent over a range of field strengths. We concluded that at the present time it is useful to analyze ER data using the FKA theory, considering the matrix element thus obtained as exciton enhanced. The FKA fits determined the E_0 gap energy to be 1.427 ± 0.003 eV (at 0 °C); the spin-orbit splitting at Γ, $\Delta_0 = 0.336 \pm 0.013$ eV. The interface between light- and heavy-hole transitions at E_0 was seen and the following quantities determined: light-hole reduced mass $\mu_{lh} = (0.030 \pm 0.005)m_e$, heavy-hole reduced mass $\mu_{hh} = (0.062 \pm 0.015)m_e$, and dipole matrix elements $C_{0\,lh} = (1.16 \pm 0.2)\hbar/a_0$, $C_{0\,hh} = (0.6 \pm 0.1)\hbar/a_0$, and $C_{0\,soh} = (0.66 \pm 0.1)\hbar/a_0$.

At the higher-energy structures, E_1, $E_1+\Delta_1$, it was found that the two-dimensional FKA theory best represented the line shapes. These transitions were attributed to transitions all along a critical line extending approximately 70% of the way along Λ from L towards Γ. The E_1 energy was found to be 2.884 ± 0.012 eV (at 0 °C) and the spin-orbit splitting $\Delta_1 = 0.227 \pm 0.010$ eV. The transverse reduced mass was determined to be $\mu_t^{2D} = 0.053m_e$ $(+0.016m_e, -0.012m_e)$.

Two structures were seen in the 4.0–5.3-eV photon energy range. The first of these, E_0', has many oscillations, but remains poorly understood. The second structure, E_2, is compatible with a one-dimensional critical-point theory as some band calculations have indicated it sould be. However, the structure is so broad that it can also be fit with other types of FKA line shapes. The M_0^{1D} theory places the critical-point energy at $E_2 = 4.95 \mp 0.020$ eV (at 0 °C) and indicates that the critical plateaus responsible have a total effective area on the order of 0.18 $(1/a_0)$ per Brillouin zone.

*Work supported in part by the Advanced Research Projects Agency under Contract No. HC 15-67-C-0221, the U.S. Army Research Office, Durham under Contract No. DA-HC04-67-0025, and the Office of Naval Research.

†Present address: Xerox Research Laboratories, Xerox Square, W114, Rochester, N.Y. 14644.

[1]Stephen F. Pond and Paul Handler, Phys. Rev. B 6, 2248 (1972).
[2]B. O. Seraphin and N. Bottka, Phys. Rev. **145**, 628 (1966).
[3]A. Frova and D. E. Aspnes, Phys. Rev. **182**, 795 (1969); D. E. Aspnes and A. Frova, Solid State Commun. 7, 195 (1969).
[4]S. Koeppen and P. Handler, Phys. Rev. **187**, 1182 (1969).
[5]Y. Hamakawa, F. A. Germano, and P. Handler, Phys. Rev. **167**, 703 (1968).
[6]R. A. Forman, D. E. Aspnes, and M. Cardona, J. Phys. Chem. Solids **31**, 227 (1970).
[7]Y. Hamakawa, F. A. Germano, and P. Handler, J. Phys. Soc. Jap. Suppl. **21**, 111 (1966).
[8]D. F. Blossey, Phys. Rev. B **2**, 3976 (1970); Phys. Rev. B **3**, 1382 (1971).

[9]F. C. Weinstein, J. D. Dow, and B. Y. Lao, Phys. Rev. B **4,** 3502 (1971).
[10]Victor Rehn and D. S. Kyser, Phys. Rev. Lett. **18,** 848 (1967).
[11]N. Bottka and J. E. Fischer, Phys. Rev. B **3,** 2514 (1971).
[12]D. E. Aspnes, Phys. Rev. Lett. **28,** 913 (1971).
[13]J. Grover, S. Koeppen, and P. Handler, Phys. Rev. B **4,** 2830 (1971).
[14]D. E. Aspnes, Phys. Rev. **147,** 554 (1966); Phys. Rev. **153,** 972 (1967).
[15]M. Cardona, Solid State Phys. Suppl. **11,** 67 (1967).
[16]R. C. Eden, Ph.D. thesis (Stanford University, 1967) (unpublished). (Available through University Microfilm Library Service, Xerox Corp., Ann Arbor, Mich. 48106 as item 67-17415, R.C. Eden.)
[17]M. A. Gilleo and P. T. Bailey, Phys. Rev. **187,** 1181 (1969).
[18]A fit was performed on the data of Ref. 19 by following the procedure described by D. D. Sell and P. Lawaetz, Phys. Rev. Lett. **26,** 311 (1962). The 21 °K data were used and the fitting parameters were exciton rydberg, 42 meV; broadening, 3.1 meV; energy gap, 1.522 eV; and effective reduced mass, $0.048m_e$.
[19]R. J. Elliot, Phys. Rev. **108,** 1384 (1957).
[20]M. Sturge, Phys. Rev. **127,** 768 (1962).
[21]Actually the room-temperature gap energy was computed as was the liquid-nitrogen gap energy. We then extrapolated linearly to 0 °C.
[22]J. Wells and P. Handler, Phys. Rev. B **3,** 1315 (1971). Wells and Handler determined a room-temperature gap energy of 1.425 eV. This corresponds to a 0 °C energy for the gap of 1.432 eV.
[23]Q. H. F. Vehren, J. Phys. Chem. Solids **29,** 129 (1968).
[24]M. Reine, J. Aggarwal, and B. Lax, Phys. Rev. B **2,** 458 (1970).
[25]M. Cardona, K. L. Shaklee, and F. H. Pollak, Phys. Rev. **154,** 696 (1967).
[26]R. W. Shaw, Phys. Rev. B **3,** 3283 (1970).
[27]D. E. Aspnes and A. Frova, Phys. Rev. B **2,** 1037 (1970); Phys. Rev. B **3,** 1511E (1971).
[28]Equation (12) of the paper by E. O. Kane, J. Phys. Chem. Solids **1,** 249 (1957) was used with the conduction-band mass found in Ref. 22 and our values for the energy-gap and spin-orbit splitting at Γ to compute $C_0 = 0.38\hbar/a_0$.
[29]D. F. Blossey, Ph.D. thesis (University of Illinois, 1969) (unpublished).
[30]J. C. Phillips, J. Phys. Chem. Solids **12,** 208 (1960).
[31]D. Brust, J. C. Phillips, and F. Bassini, Phys. Rev. Lett. **9,** 94 (1962).
[32]D. Brust, Phys. Rev. **134,** A1337 (1964).
[33]R. F. Potter, Phys. Rev. **150,** 562 (1966).
[34]D. L. Greenaway and M. Cardona, *Proceedings of the International Conference on the Physics of Semiconductors, Exeter, England*, (Institute of Physics and the Physical Society, London, 1962),,p. 666.
[35]D. D. Sell and S. E. Stowkowski, *Proceedings of the International Conference on the Physics of Semiconductors, Cambridge, Mass.*, AEC Technical Publication No. CONF-700801 (U. S. AEC, Oak Ridge, Tenn., 1970), p. 411.
[36]G. Dresselhaus and M. S. Dresselhaus, Phys. Rev. **160,** 649 (1967).
[37]R. R. L. Zucca, J. P. Walter, Y. R. Shen, and M. L. Cohen, Solid State Commun. **8,** 627 (1970).
[38]D. E. Aspnes and J. Rowe, Ref. 35, p. 422.
[39]D. Brust, in *Methods of Computational Physics*, edited by B. Adler, S. Fernbach, and M. Rotenberg (Academic, New York, 1968), Vol. 8, p. 33.
[40]E. O. Kane, Phys. Rev. **180,** 852 (1969).
[41]S. Pond, Ph.D. thesis (University of Illinois, 1971) (unpublished).
[42]S. Koeppen, P. Handler, and S. Jasperson, in Ref. 35, p. 411.
[43]S. Koeppen, P. Handler, and S. Jasperson, Phys. Rev. Lett. **27,** 265 (1971); Phys. Rev. Lett. **27,** 1250(E) (1971).
[44]J. E. Rowe and D. E. Aspnes, Phys. Rev. Lett. **25,** 162 (1970).
[45]J. P. Walter and M. L. Cohen, Phys. Rev. **183,** 763 (1969).
[46]R. N. Cahn and M. L. Cohen, Phys. Rev. B **1,** 2569 (1970).
[47]M. Cardona and F. H. Pollak, in *Physics of Opto-Electronic Materials*, edited by W. A. Albers, Jr., General Motors Symposium Series (Plenum, New York, 1971), p. 81.
[48]R. R. L. Zucca and Y. R. Shen, Phys. Rev. B **1,** 2668 (1970).
[49]V. Rehn and D. S. Kyser, Surf. Sci. (to be published).